Engineering Science & Technology
http://ojs.wiserpub.com/index.php/EST/

UNIVERSAL WISER PUBLISHER

Research Article

Combustion Characteristics and Flame Stability of a Methane-Air Mixture in Micro-Structured Systems

Junjie Chen

Department of Energy and Power Engineering, School of Mechanical and Power Engineering, Henan Polytechnic University, Jiaozuo, Henan, P.R. China
Email: cjjtpj@163.com

Received: 3 January 2022; **Revised:** 17 February 2022; **Accepted:** 4 March 2022

Abstract: Cavities are effective in improving the ability of a flame in micro-structured systems, but the mechanism for increased flame stability remains unclear. Numerical simulations are performed to understand the overall small-scale combustion characteristics of a cavity-stabilized burner. The effects of inlet velocity, equivalence ratio, wall thermal conductivity, channel height, and heat transfer coefficient on flame stability are investigated. A dimensionless number analysis is performed to better understand the heat transfer characteristics of the burner. The results indicate that the cavity structure can induce recirculation of hot products, thereby improving flame stability. The wall thermal conductivity and inlet velocity are vital in determining the flame stability of the burner. Further improvement in flame stability can be achieved using anisotropic walls. Fast flows can cause a blowout and slow flows can cause extinction. There exists an optimum inlet velocity for the greatest flame stability. A critical issue of fuel-rich cases is the loss of combustion efficiency. Combustion at the microscale can offer many advantages. Faster ignition and more efficient heat transfer can be achieved, but the design is challenging due to the loss of flame stability.

***Keywords*:** combustion characteristics, flame stability, thermal management, burner design, heat transfer, computational fluid dynamics

1. Introduction

Compact, highly mobile, and efficient thermodynamic and energy systems are becoming increasingly important for several applications [1], [2], such as thermodynamic cycling of distributed ventilation and heating systems, modular propulsion and control of self-powered and distributed sensor and actuation systems [3], [4], cooling and powering of portable medical, communications, and electronics devices [5], [6], and many other applications. Generally, such applications optimally require cost-effective power sources, which are characterized by high energy density and power [7], [8], but minimal weight and dimensions.

Micro-structured combustion systems may overcome the limitations of traditional thermodynamic and power sources [9], [10] by providing micromachinery components that enable efficient operation of thermodynamic systems and production of significant power in the regime of millimeters [11], [12] to meet the cost, weight, modularity, mobility, and efficiency requirements of several modern applications. For example, micro-structured combustion

DOI: https://doi.org/10.37256/est.3220221321

systems can provide power sources that can be employed in various portable electric power applications [13], [14] such as portable coolers, heaters, communication and electronic devices, and other such applications.

More particularly, micro-structured combustion systems enable the realization of a wide range of micro-machinery componentry for thermodynamic cycling, propulsion, and producing sources of power that achieve high efficiencies of components [15], [16]. Micro-heat exchangers [17], [18], micro-turbines, micro-combustors [19], [20], and other micro-componentry can be developed as thermodynamic micro-modules that could be interconnected in various combinations to construct micro-structured thermodynamic cycles such as micro-gas turbine generators [21], [22], micro-gas turbine engines [23], [24], and a wide range of other thermodynamic cycles [25], [26] in the regime of millimeters. Specifically, micro-structured combustion systems apply to all portable electric power applications for which air is available [27], [28]. The very low noise produced by micro-structured combustion systems makes them particularly attractive from a practical perspective for applications such as military reconnaissance and office electronics [29], [30]. Micro-structured combustion systems can be further advantageously employed in manned mobile scenarios [31], [32]. Micro-structured combustion systems can similarly be employed to power implanted medical devices, for example, pacemakers.

Unfortunately, flame stabilization is a common problem in micro-structured combustion systems [33], [34]. Hydrocarbon flames are typically quenched when confined within spaces with critical dimensions less than 2 mm, depending on the flow velocity, composition, and geometry [35], [36]. Flames are quenched in these small dimensions due to two primary mechanisms, including thermal and radical quenching. When sufficient heat is removed through the walls, combustion cannot be self-sustained and thermal quenching occurs [37], [38]. Radical quenching occurs through the adsorption of radicals on the walls and subsequent recombination, which can lead to a lack of homogeneous chemistry [39], [40]. The small scales of micro-structured combustion systems make them significantly more prone to both quenching mechanisms [41], [42] due to the high surface area-to-volume ratios, which will lead to increased radical mass transfer and enhanced heat transfer from the flame to the walls. In addition to flame quenching, a blowout can occur when the burner exit velocity exceeds the flame burning velocity [43], [44]. In this mechanism, the reaction shifts downstream until it exits the burner.

To achieve improvements in flame stability, various methods have been tried either commercially or experimentally [45], [46] and different structures have already been designed for micro-structured combustion systems [47], [48]. The typical method includes the use of recirculation regions to provide a continuous ignition source by mixing the hot combustion products with the cold incoming fuel and air mixture. Structural devices have been commonly employed to establish a recirculation region for improving the stability of the flame during ignition and operation, for example, cavities [49], [50]. A fundamental understanding of the stabilization mechanisms of a flame within very small spaces by the cavity method is of both fundamental and practical significance. However, the precise mechanism by which the cavity method generally provides increased flame stability remains unclear and warrants further study.

This study relates to the combustion characteristics of a micro-structured cavity-stabilized burner. Simulations are conducted to gain insights into burner performance such as reaction rates, species concentrations, temperatures, and flames. The factors affecting combustion characteristics are determined for the cavity-stabilized burner. Particular focus is on determining essential factors that affect the performance of the burner.

2. *Description of the model*

2.1 *Description of the combustion system*

The use of a cavity configuration is particularly advantageous when arranged as a disturbance factor for a millimeter-scale burner. The millimeter-scale burner designed with cavities is depicted schematically in Figure 1. A lean methane-air mixture is conducted through a combustion chamber defined by parallel plates. The length of the channel is 50 mm, the height is 3 mm, and the width is 13 mm. The depth of the cavities is 1.5 mm, the width of the cavities is 4 mm, and the distance away from the entrance is 10 mm. The angle of the cavity is 45 °, and the thickness of the plates is 3 mm, as depicted schematically in Figure 1. The initial temperature is 1,500 K, with a Reynolds number greater than 500 at the inlet. Due to the small internal space of the burner, the gas flow rate is small. Therefore, gas radiation and volume forces are ignored in the model.

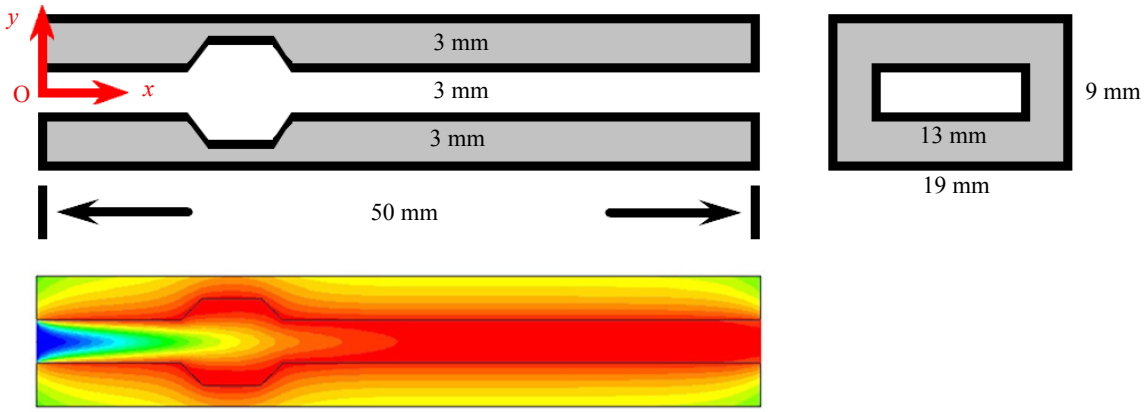

Figure 1. Schematic illustration of the millimeter-scale combustion system designed with cavities on the channel walls

2.2 *Mathematical model*

The mathematical model is solved and implemented in ANSYS FLUENT to obtain the problem solution. ANSYS FLUENT permits multi-dimensional modeling of physical and chemical phenomena in the processes [51], [52], and various modes of heat transfer can be modeled.

Continuity equation:

$$\frac{\partial}{\partial x}\left(\rho \upsilon_x\right)+\frac{\partial}{\partial y}\left(\rho \upsilon_y\right)=0, \tag{1}$$

where υ is the velocity, ρ is the density, and x and y denote Cartesian coordinates.

Momentum conservation equations:

$$\frac{\partial\left(\rho \upsilon_x \upsilon_x\right)}{\partial x}+\frac{\partial\left(\rho \upsilon_x \upsilon_y\right)}{\partial y}=-\frac{\partial p}{\partial x}+\frac{\partial \tau_{xx}}{\partial x}+\frac{\partial \tau_{xy}}{\partial y}, \tag{2}$$

$$\frac{\partial\left(\rho \upsilon_y \upsilon_x\right)}{\partial x}+\frac{\partial\left(\rho \upsilon_y \upsilon_y\right)}{\partial y}=-\frac{\partial p}{\partial y}+\frac{\partial \tau_{yx}}{\partial x}+\frac{\partial \tau_{yy}}{\partial y}, \tag{3}$$

where τ is the stress tensor.

Energy conservation equation:

$$\frac{\partial\left(\rho \upsilon_x h\right)}{\partial x}+\frac{\partial\left(\rho \upsilon_y h\right)}{\partial y}=\frac{\partial\left(k_f \partial T\right)}{\partial x^2}+\frac{\partial\left(k_f \partial T\right)}{\partial y^2}+\sum_i\left[\frac{\partial}{\partial x}\left(h_i \rho D_i \frac{\partial Y_i}{\partial x}\right)+\frac{\partial}{\partial y}\left(h_i \rho D_i \frac{\partial Y_i}{\partial y}\right)\right]+\sum_i h_i R_i, \tag{4}$$

where h is the enthalpy, k is the thermal conductivity, T is the temperature, Y is the mass fraction, D is the molecular diffusivity, R is the reaction rate, and f denotes the fluid.

Species conservation equation:

$$\frac{\partial\left(\rho Y_i \upsilon_x\right)}{\partial x}+\frac{\partial\left(\rho Y_i \upsilon_y\right)}{\partial y}=\frac{\partial}{\partial x}\left(\rho D_{i,m} \frac{\partial Y_i}{\partial x}\right)+\frac{\partial}{\partial y}\left(\rho D_{i,m} \frac{\partial Y_i}{\partial y}\right)+R_i. \tag{5}$$

Solid energy conservation equation:

$$\frac{\partial}{\partial x}\left(k_s \frac{\partial T}{\partial x}\right)+\frac{\partial}{\partial y}\left(k_s \frac{\partial T}{\partial y}\right)=0. \tag{6}$$

where *s* denotes the solid walls.

2.3 *Chemical kinetic model*

The species involved in the combustion reaction need to be explicitly specified in ANSYS FLUENT. The reaction is defined in ANSYS FLUENT by setting a stoichiometric coefficient and a rate exponent for each reactant and product. Additionally, the parameters for the Arrhenius rate are also specified in ANSYS FLUENT, including the pre-exponential factor, activation energy, and temperature exponent of the reaction.

The reaction rate expression can be written as follows [53]:

$$r_{CH_4}\left[\text{kmol}\cdot\text{m}^{-3}\cdot\text{s}^{-1}\right]=2.119\times10^{11}\cdot\exp\left[-\frac{2.027\times10^{8}}{RT}\right]\cdot\left[CH_4\right]^{0.2}\cdot\left[O_2\right]^{1.3}, \tag{7}$$

where the unit of reaction rate is the kmol/(m^3·s), the unit of activation energy is J/kmol, and the unit of concentration is kmol/m^3. This chemical kinetic model can be used to accurately describe flame dynamics and flame responses to external perturbations [54]. Thermal effects can be relatively well captured by the chemical kinetic model.

The chemical kinetic model used is simple but effective and efficient, thereby significantly reducing the cost and time of computation. The model is widely used for chemically reactive systems involving methane flames. GRI-Mech is specifically designed to describe methane and ethane combustion and is limited to high-temperature phenomena. GRI-Mech has been an enormous success and positive addition to the computational modeling tools available to researchers. The extra computational costs of using GRI-Mech may be worth investing in to analyze the complex problem. However, numerical convergence is in general difficult due to the inherent stiffness of the kinetic equations. Differential equations are written for the concentration of each chemical species in the system being studied. These coupled equations frequently have widely disparate characteristic time scales, referred to as stiffness. To achieve convergence and to compute extinction points, the one-step approximation described above is used for the chemically reactive system.

2.4 *Design parameters*

Table 1. Design parameters of the millimeter-scale cavity-stabilized combustion systems used in the computational fluid dynamics modeling

Variables	Inlet velocity (m/s)	Equivalence ratio	Thermal conductivity (W/(m·K))	Channel height (mm)	Heat transfer coefficient (W/(m^2·K))
Effect of thermal conductivity	0.3	1.0	0.5, 1.4, 50, 50-0.5, 200	3	10
Effect of equivalence ratio	0.3	0.4, 0.6, 0.8, 1.0, 1.2	1.4	3	10
Effect of inlet velocity	0.1, 0.3, 0.5, 0.7	1.0	1.4	3	10
Effect of heat transfer coefficient	0.3	1.0	1.4	3	10, 20, 40, 60
Effect of channel height	0.3	1.0	1.4	3, 4, 5	10

The design parameters of the burner are summarized in Table 1. To avoid a negative effect on the combustion

conditions, the design parameters must be selected with respect to each other in such a way that the highest stability is achieved for the methane flame. The influences of the design parameters are investigated by varying a particular design parameter while maintaining the other design parameters. Hereinafter, the parameters used are given in Table 1, unless otherwise stated.

2.5 *Mesh independence test*

The typical mesh used for the cavity-stabilized burner is illustrated in Figure 2. More nodes are accumulated around the cavity structure and the reaction regions. In total, the typical mesh consists of 36,000 nodes for the cavity-stabilized burner. A mesh independence test is performed to assure the independence of the solution. The fluid centerline temperature profiles are presented in Figure 3 for meshes with different nodal densities. The inlet velocity of the gases is 0.6 m/s, with a stoichiometric fuel-air ratio. As the mesh density increases, there is a convergence of the solution. Solutions obtained with a mesh consisting of 36,000 nodes are reasonably accurate. Larger mesh densities, up to 72,000 nodes, offer no obvious advantage.

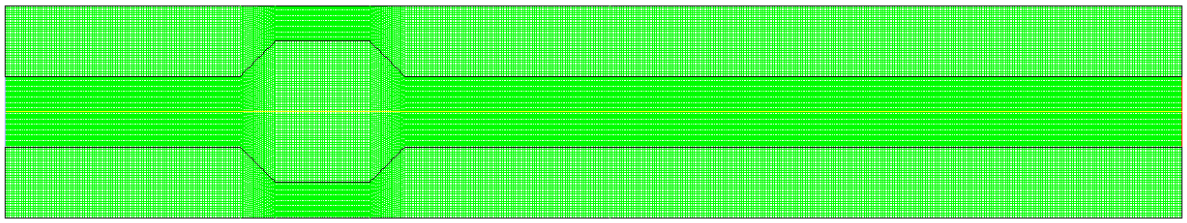

Figure 2. Typical mesh used for the cavity-stabilized burner. More nodes are placed around the cavity structure and the reaction regions

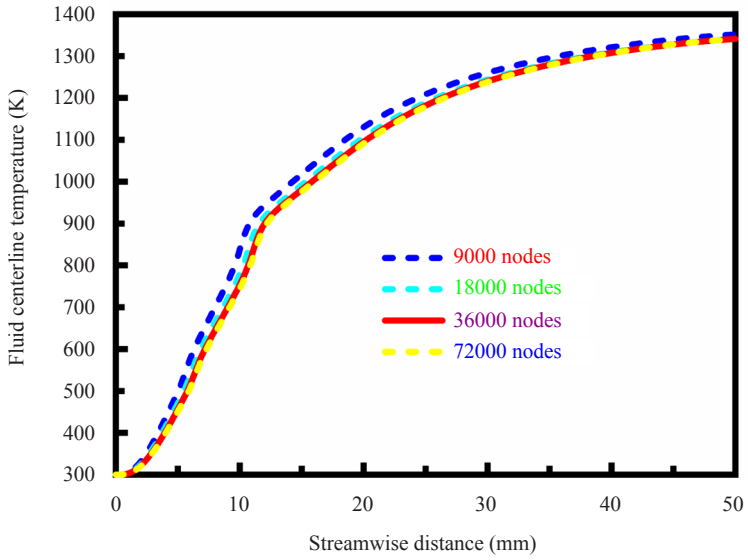

Figure 3. Fluid centerline temperature profiles for meshes with different nodal densities. The inlet velocity of the gases is 0.6 m/s, with a stoichiometric fuel-air ratio

2.6 *Validation of the model*

To verify the accuracy of the model, the predictions are compared with the data obtained from experimental measurements. The burner comprises two parallel fused-quartz plates. An ordinary camera is used to form an image

using visible light, and a thermographic camera is used to create an image using infrared radiation. The thermographic camera can achieve a resolution of 640 × 480 pixels, and a temperature difference of 1.0 K at the scene induces a maximum temperature difference of 0.02 K at the sensor. The stable fluid centerline temperature profiles are determined from thermographic measurements using infrared radiation. A constant fuel-air stoichiometry is maintained in operation. The thermographic images acquired in the infrared spectral region, and the optical images in the visible spectral region, are presented in Figure 4. The contour plot of temperature in the burner is also presented in Figure 4. The fluid centerline temperature is plotted in Figure 5 against the streamwise distance. The fluid centerline temperature profiles are determined from thermographic measurements and predicted by the model. The predictions are in satisfactory agreement with the data obtained from experimental measurements.

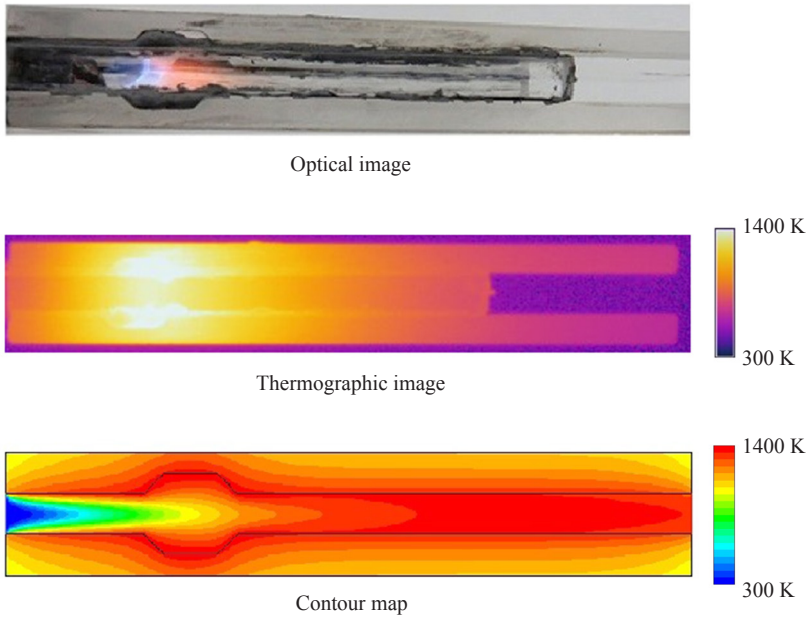

Figure 4. Laminar premixed methane flames and temperature variation in the burner. A constant fuel-air stoichiometry is maintained in operation

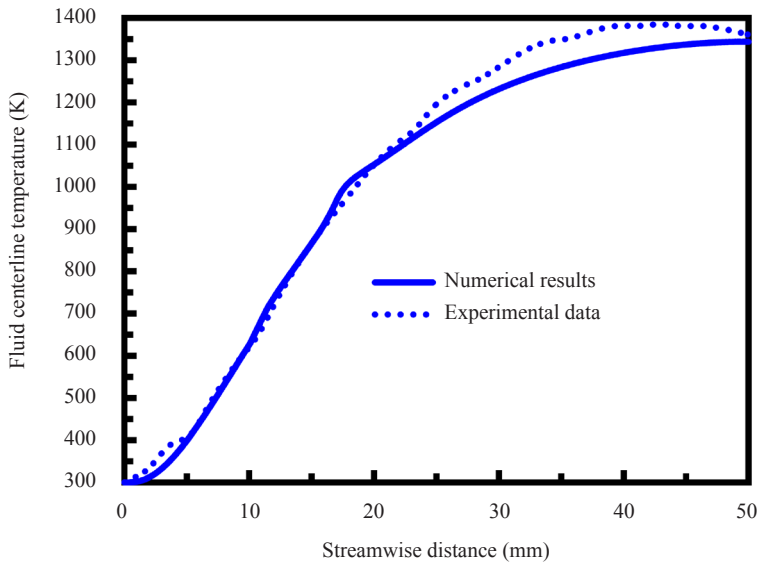

Figure 5. Fluid centerline temperature profiles are determined from thermographic measurements and predicted by the model. A constant fuel-air stoichiometry is maintained in operation

2.7 *Classification of combustion instabilities*

Combustion instability can be classified into three categories [55], [56]: chamber, intrinsic, and system instabilities.

• Chamber instability arises due to the occurrence of combustion inside a chamber, such as fluid-dynamic instability, shock instability, and acoustic instability.

• Intrinsic instability arises irrespective of whether combustion occurs inside a chamber or not, such as hydrodynamic instability, diffusive-thermal instability, and chemical-kinetic instability.

• System instability arises due to the interaction between combustion processes in the chamber and anywhere else in the system, such as feed-system interactions and exhaust-system interactions.

Intrinsic instability may arise when the physicochemical balances associated with the propagation of a flame are offset [57], [58]. In a premixed flame, the primary mechanism for loss of stability is hydrodynamic instability, which is often referred to as the Darrieus-Landau instability, due to the thermal expansion of the gas produced by the combustion process [59], [60]. The flame front is unstable to perturbations of any wavelength. In a non-premixed flame, thermo-diffusive instability is predominant while hydrodynamic instability plays a secondary role.

The present study is focused primarily on extinction and blowout. A flame is quenched in a small space due to two primary mechanisms: thermal and radical quenching. Thermal quenching occurs when sufficient heat is removed through the walls. Radical quenching occurs via the adsorption of radicals on the system walls and subsequent recombination, which will lead to a lack of homogeneous chemistry. Another mechanism for loss of stability is a blowout, which occurs when the burner exit velocity exceeds the flame burning velocity. The propagation speed of a premixed flame is referred to as the flame speed or burning velocity. Laminar flame speed is an intrinsic characteristic of premixed combustible mixtures. The experimentally determined laminar flame speed is about 0.38 m/s for a stoichiometric methane-air mixture at room temperature [61], [62]. In this mechanism, the reaction front shifts downstream with increasing flow velocity and eventually exits the burner.

3. Results and discussion

3.1 *Performance comparison*

Before performing the computation, a comparison of methane conversion rate is carried out between a flat-plate burner and a cavity-stabilized burner. The composition change of the flat-plate burner and the cavity-stabilized burner is determined under the conditions of an equivalent ratio of 1.0, an inlet velocity of 0.5 m/s, and a wall thermal conductivity of 0.7 W/(m·K). The results are present in Figure 6, in which the axial fluid centerline temperature and the methane mass fraction are plotted against the streamwise distance. The methane conversion rate of the flat-plate burner is about 30%, and the methane conversion rate of the cavity-stabilized burner is about 90%. Therefore, the combustion efficiency of methane in the cavity-stabilized burner is higher than that of methane in the flat-plate burner. More complete combustion can be achieved in the cavity-stabilized burner. Even after ignition, it is difficult to maintain stable combustion in the flat-plate burner.

When the cavity structure is formed, a recirculation region is established for the cavity-stabilized burner. As a result, the methane mass fraction is small at the outlet, and the axial fluid centerline temperature is higher than that in the flat-plate burner. Therefore, the cavity structure is important for improving operation, and the cavity-stabilized burner operates at a substantially higher temperature than the flat-plate burner. The contour plots of temperature are illustrated in Figure 7 for the flat-plate and cavity-stabilized burners. An important feature of the cavity-stabilized burner is that high enough flame temperatures are achievable to permit effective use of the fuel, thereby raising the temperature to about 1,400 K, which is much higher than that in the flat-plate burner. Since temperature and reaction rate are functionally related, an increase in temperature will lead to a corresponding increase in the reaction rate. As a result, rapid, efficient thermal combustion occurs in the cavity-stabilized burner. Combustion of the methane-air mixture is stabilized in the cavities. The combustion region is maintained downstream of the cavity structure, which is capable of creating a recirculation region to provide heat to the mixture either through conduction or radiation. This differs from the flat-plate burner in which the cavities are absent. Advantageously, the cavity structure is useful for flame stabilization applications. The temperature increases when cavity stabilization is used. Combustion is stabilized by recirculation of

hot combustion products induced by the cavity structure. However, the cavity-stabilized burner has practical limits in terms of the cavity structure, since complexity is introduced into the design of the cavity-stabilized burner.

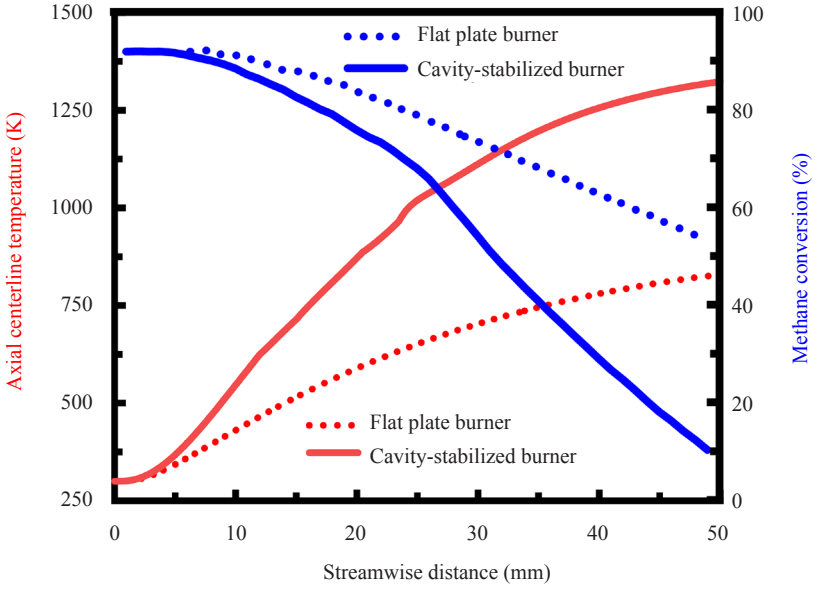

Figure 6. Axial fluid centerline temperature and methane mass fraction profiles along the length of the flat-plate and cavity-stabilized burners

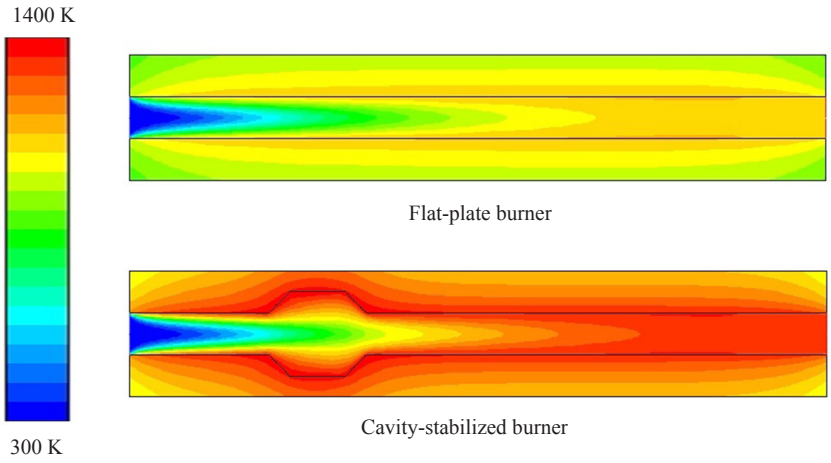

Figure 7. Contour plots of temperature for the flat-plate and cavity-stabilized burners. At room temperature, the thermal conductivity of the burner walls is 1.4 W/(m·K)

3.2 *Effect of inlet velocity*

The effect of changes in inlet velocity on burner temperature changes is investigated, and the axial fluid centerline temperature profiles are presented in Figure 8. Additionally, the effect of changes in velocity on methane conversion is illustrated in Figure 9. As the velocity increases, the residence time of the fuel in the burner becomes shorter. As the velocity increases, the position of the ignition point of the burner gradually moves away from the inlet to the outlet, as shown in Figure 8. This will lead to raise the temperature to about 1,400 K, which may lead to the formation of nitrogen oxides.

The methane conversion rate increases with the velocity, as shown in Figure 9, thereby stabilizing combustion.

Combustion is more readily stabilized in the cavity-stabilized burner at low velocities. Blowout will occur at sufficiently high velocities [63], [64]. Therefore, an appropriate velocity is very important for the continued stabilization of combustion in the burner. Cavity-stabilized combustion will tend to reduce unburned hydrocarbons emissions, as shown in Figure 9. Consequently, the velocity is a critical factor in assuring flame stability within the cavity-stabilized burner.

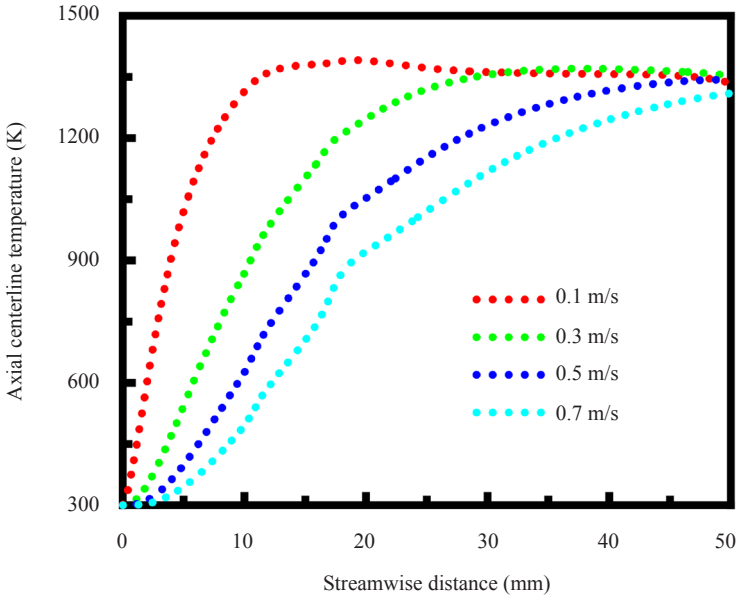

Figure 8. Axial fluid centerline temperature profiles along the length of the cavity-stabilized burner under different methane-air mixture inlet velocity conditions

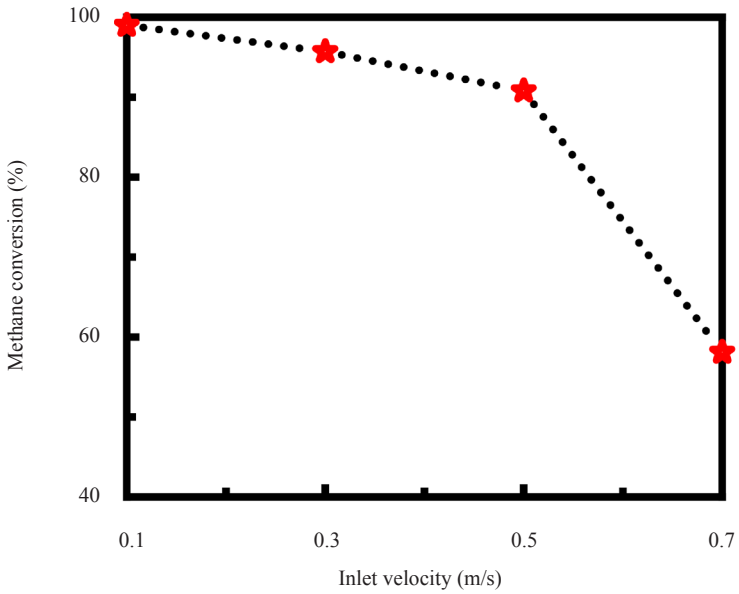

Figure 9. Effect of methane-air mixture inlet velocity on the methane conversion at the outlet of the cavity-stabilized burner

The axial centerline reaction rate profiles are presented in Figure 10 at different inlet velocities. As the velocity increases, the peak of the reaction rate along the axis gradually moves away from the inlet to the outlet. When the

velocity is low, methane is substantially completely converted near the inlet, and the peak of the reaction rate is also close to the inlet. When the velocity is high, the flame shifts toward the outlet, and the fuel fails to fully react with air, as shown in Figure 10. In this case, the peak of the reaction rate is closer to the outlet. For fast flows, blowout occurs, whereas for slow flows, global type extinction occurs due to slow convective heat transfer. As a result, there exists an optimum inlet velocity for the highest reaction rate, which is 0.3 m/s for the conditions studied here.

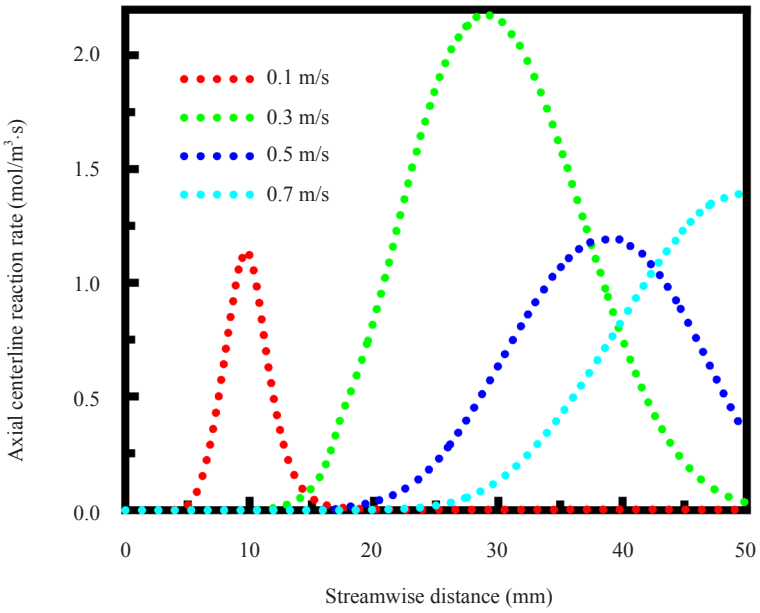

Figure 10. Axial centerline rate profiles of the combustion reaction in the cavity-stabilized burner under different methane-air mixture inlet velocity conditions

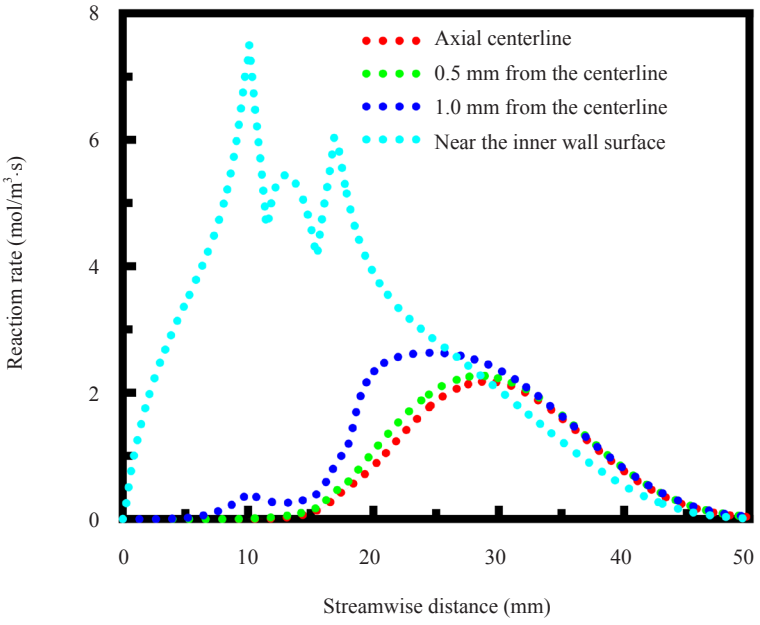

Figure 11. Transverse rate profiles of the combustion reaction at different distances from the axial centerline. The methane-air mixture inlet velocity is 0.3 m/s

The transverse rate profiles of the combustion reaction are presented in Figure 11 at different distances from the axial centerline. The velocity is 0.3 m/s. When the distance from the axial centerline is 0.5 mm and 1.0 mm, the peak of the reaction rate generally occurs near the middle of the cavity-stabilized burner. When the position is near the inner wall surface, the peak of the reaction rate is close to the entrance. This is because when the velocity is low, the wall temperature is higher than the temperature of the central flow channel, and the gas near the wall can quickly absorb heat and reach the ignition temperature to react. The irregular change of the rate of the combustion reaction near the cavities is mainly due to the formation of low-speed recirculation regions, in which the heat and mass transfer in the cavities are uneven. Advantageously, the recirculation regions make the gas in the cavities flow violently, which facilitates the combustion process.

3.3 *Effect of channel height*

The major problem of the micro-structured burner is the high ratio of surface to volume [65], [66]. As the ratio of surface to volume increases, heat loss to the surroundings increases, which could eventually lead to flame quenching [67], [68]. Therefore, the effect of the dimensions of the burner, for example, channel height, is investigated to better understand the stability of flame in the cavity-stabilized burner. The change characteristics of the temperature along the outer wall surface of the burner and the axial centerline are presented in Figure 12 under different channel height conditions. As the height of the burner channel increases, the temperature of the axial centerline of the burner decreases, and the ignition position of the flame is far away from the inlet position, which further reduces the combustion efficiency. As the height of the burner channel increases, the temperature of the outer wall increases. This is because, under the same conditions such as a flow velocity of 0.3 m/s and an equivalent ratio of 1.0, the amount of methane flowing into the channel per unit time increases with the channel height. As a result, the heat released by fuel combustion increases, and the temperature of the outer wall surface increases. However, the combustion efficiency decreases with the channel height. As the height of the burner channel increases, the amount of unreacted fuel in the axial centerline becomes larger, and the premixed incoming fuel-air mixture will absorb more heat for preheating. As a result, the temperature of the axial centerline drops significantly.

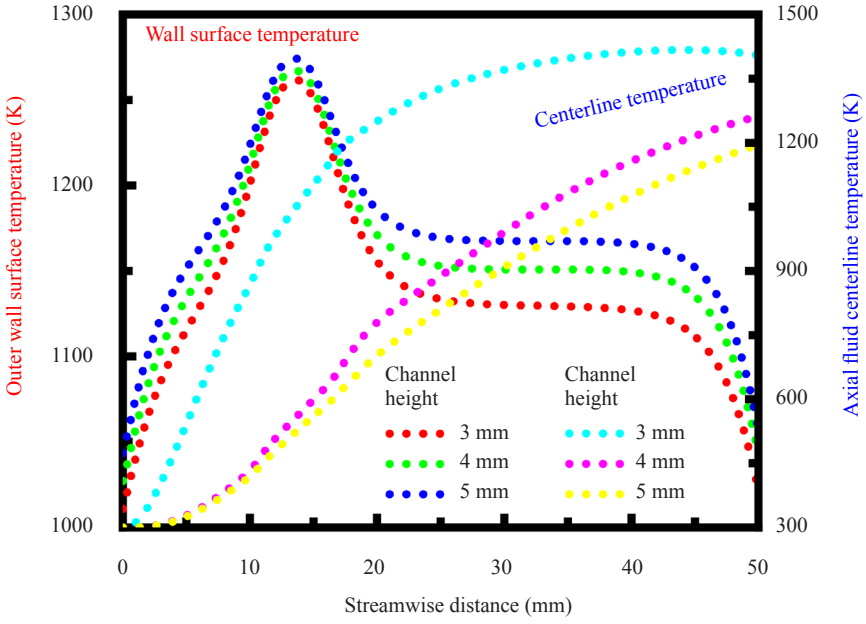

Figure 12. Temperature profiles along the outer wall surface of the cavity-stabilized burner and the axial centerline under different channel height conditions

3.4 *Effect of wall thermal conductivity*

The contour plots of temperature are presented in Figure 13 at different thermal conductivities. The thermal conductivity of the solid material has little effect on the temperature of the fluid but has a strong effect on the temperature of the walls. The temperature gradient is steep within the walls with low thermal conductivity. The temperature of the exterior walls typically increases with the thermal conductivity. The solid material is advantageously thermally conductive to permit a high wall temperature with a more uniform distribution. A portion of the heat of the reaction is transferred to the upstream structure of the burner by heat conduction through the walls, which is necessary for ignition and flame stability [63], [64]. The term anisotropy is used in Figure 13 to describe the direction-dependent thermal conductivity of the solid material. In this case, the anisotropic solid material inhibits transverse but allows longitudinal heat conduction. The walls permit heat flux in the longitudinal direction to preheat the fluid, yet do not permit heat losses in the transverse direction to the surroundings.

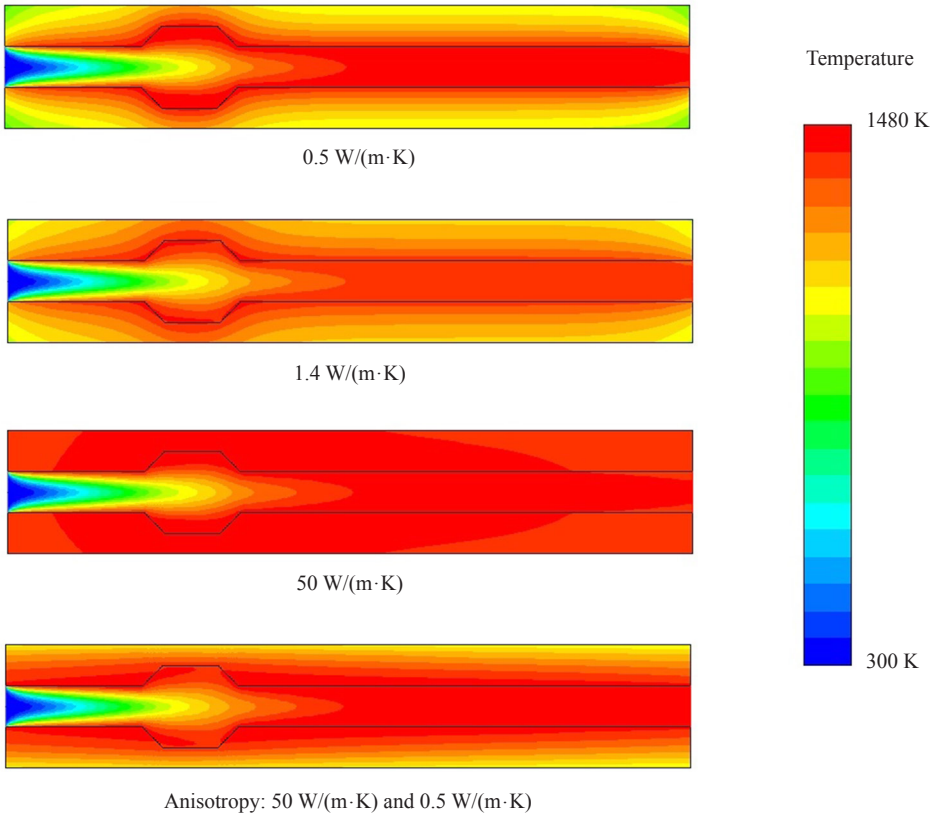

Figure 13. Contour plots of temperature at different thermal conductivities. The thermal conductivity of the anisotropic solid material is 50 W/(m × K) in the longitudinal direction and 0.5 W/(m × K) in the transverse direction

The temperature change characteristics of the outer wall surface of the burner are illustrated in Figure 14 at different thermal conductivities. As the thermal conductivity increases, the temperature of the outer wall surface increases, and the wall temperature distribution is more uniform. Ceramics with high thermal conductivity may be employed for the burner. However, the excessive temperature will cause a large amount of heat loss, which will cause unstable combustion performance. In addition, it is important to operate the burner at a safe temperature. When the thermal conductivity is low, the temperature of the outer wall surface is also low and the temperature distribution is uneven. This will be detrimental to the flame stability of the burner, and local thermal stress is prone to occur. To better solve the above problems, walls with anisotropic thermal conductivity can not only transfer heat upstream for

preheating the low-temperature unreacted pre-mixed gas but also reduce the large heat loss caused by excessive wall temperatures, which will lead to unstable combustion performance. Two-dimensional materials may have anisotropic thermal properties [69], [70], for example, graphene.

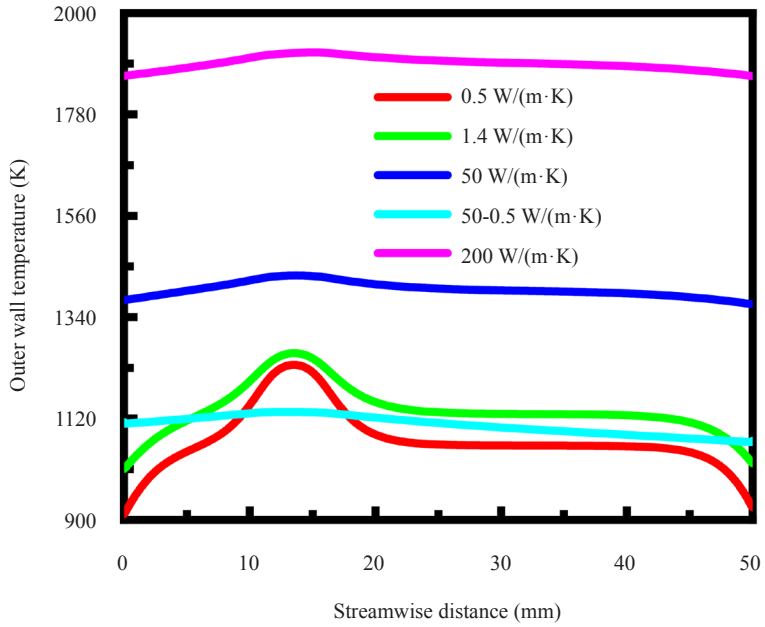

Figure 14. Temperature profiles along the outer wall surface of the cavity-stabilized burner under different thermal conductivity conditions

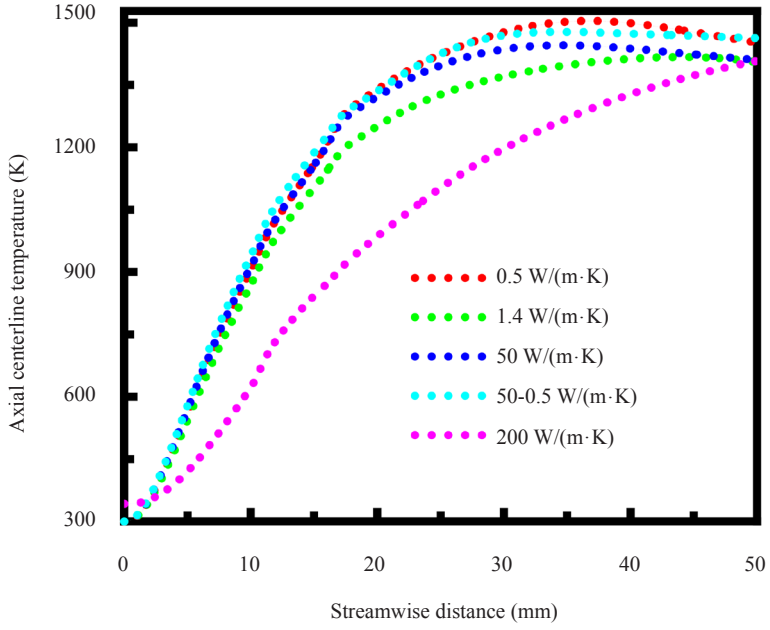

Figure 15. Temperature profiles along the axial fluid centerline of the cavity-stabilized burner under different thermal conductivity conditions

The temperature profiles along the axial fluid centerline of the cavity-stabilized burner are presented in Figure 15 at different thermal conductivities. The thermal conductivity mainly affects the temperature of the burner wall

surfaces as well as the rate of heat transfer, as discussed above. In contrast, the thermal conductivity has little effect on the temperature along the axial centerline, as shown in Figure 15. However, walls with excessively large thermal conductivity may cause unstable combustion, large heat loss, and the methane flame moves toward the outlet. Additionally, the temperature along the axial fluid centerline is relatively low when the thermal conductivity is 200 W/(m·K), as shown in Figure 15, but the temperature at the outlet is relatively high. The temperature difference is small between the different thermal conductivity cases, except the highest thermal conductivity case. Further improvements are achievable by using walls with anisotropic thermal conductivity, as discussed above.

3.5 *Effect of wall heat transfer coefficient*

The change characteristics of the temperature along the outer wall surface of the burner and the axial fluid centerline are presented in Figure 16 under different wall heat transfer coefficient conditions. As the heat transfer coefficient between the solid surface and the environment is increased, the wall heat loss increases. As a result, both the temperature of the outer wall surface of the burner and the temperature along with the axial fluid centerline decrease, which will lead to a drop in overall burner temperature, thereby reducing the combustion efficiency of the fuel. When the heat transfer coefficient between the solid surface and the environment is 10 W/(m^2·K), the highest temperatures are obtained at the outer wall surface and along the axial fluid centerline. With the increase of the heat transfer coefficient, the temperature of the outer wall surface decreases. At larger heat transfer coefficients, the drop in temperature becomes more pronounced. The difference in temperature between the axial fluid centerlines is much smaller than that in temperature between the outer wall surfaces. For example, near the cavities where the axial distance varies from 10 to 20 mm, the maximum difference is about 40 K between the axial fluid centerline temperatures, but the maximum difference is about 90 K between the outer wall surface temperatures. Therefore, the wall heat transfer coefficient has a small effect on the axial fluid centerline temperature, but it plays a considerable role in the outer wall surface temperature.

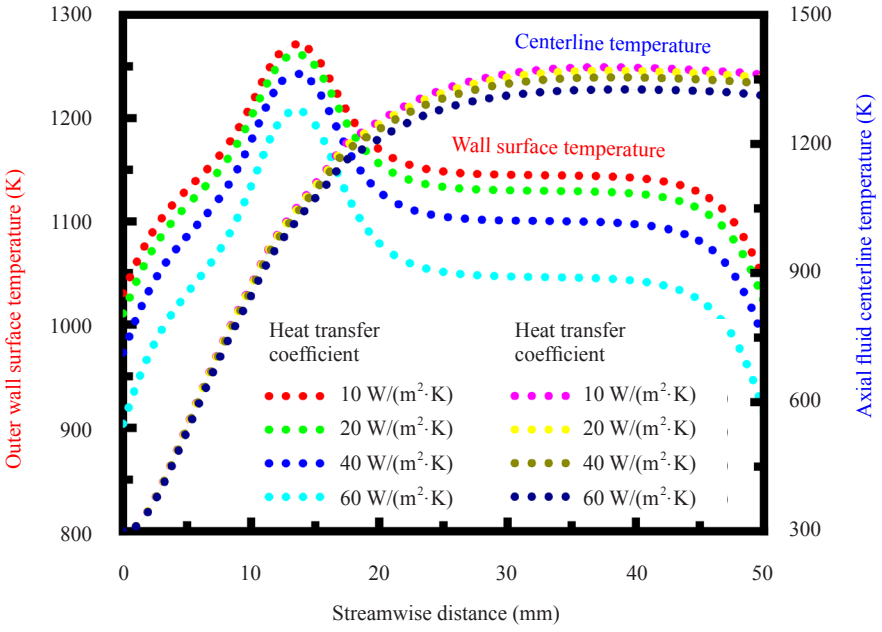

Figure 16. Temperature profiles along the outer wall surface of the burner and the axial centerline under different wall heat transfer coefficient conditions

The variation characteristics of the combustion reaction rate along the axial centerline are illustrated in Figure 17 under different wall heat transfer coefficient conditions. As the heat transfer coefficient increases, the reaction rate

decreases due to increased heat losses, especially under very lager wall heat transfer coefficient conditions. However, the peak reaction rate remains unchanged, regardless of the wall heat transfer coefficient. Therefore, losses of combustion stability because of heat losses are the main issue that requires careful management of thermal energy for the burner. A means for thermal management should be provided. From a practical viewpoint, the walls of the cavity-stabilized burner should have an anisotropic thermal conductivity. The burner walls should inhibit transverse heat conduction but allow axial heat conduction. These burner walls with anisotropic heat conduction properties will allow upstream heat flux to preheat the incoming mixture, yet not allow heat losses in the transverse direction. Alternatively, different suggestions have been made for facilitating the stability of flame in a micro-structured burner [71], [72]. To overcome the problem of heat losses involved in a micro-structured burner, catalytic combustion has been demonstrated the advantages in terms of reduced heat losses [73], [74]. This approach can substantially eliminate the formation of oxides of nitrogen [75], [76] and greatly reduce heat loss, but surface transport is still a problem. Catalytically supported thermal combustion, which is a unique combination of catalytic and gas-phase combustion, can achieve a higher stability and obtain a higher efficiency in operation than otherwise obtainable.

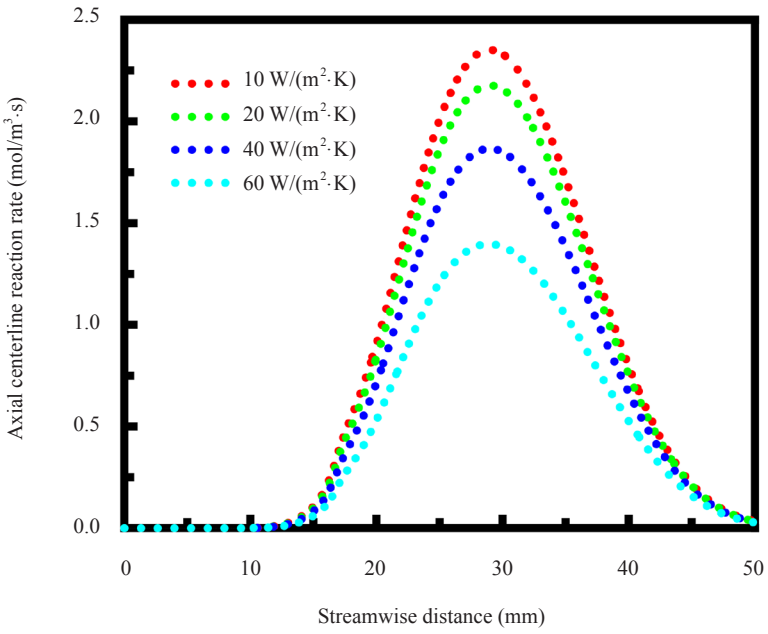

Figure 17. Axial centerline rate profiles of the combustion reaction under different wall heat transfer coefficient conditions

3.6 *Effect of fuel-air equivalent ratio*

The temperature profiles along the outer wall surface of the burner and the axial fluid centerline are presented in Figure 18 under different fuel-air equivalent ratio conditions. As the fuel-air equivalent ratio increases from 0.6 to 1.0, both the temperature along the axial fluid centerline and the temperature along the outer wall surface gradually increase. The amount of heat released by the combustion reaction increases due to the increased amount of methane gas flowing into the burner. This is because when the fuel-air equivalent ratio is less than 1.0, the amount of the methane gas flowing into the burner per unit time is smaller than that in the case of complete combustion in which the equivalence ratio is 1.0. However, when the fuel-air equivalent ratio is increased from 1.0 to 1.2, both the temperature along the axial fluid centerline and the temperature along with the outer wall surface decrease. This is because when the fuel-air equivalent ratio is greater than 1.0, the amount of the methane gas flowing into the burner per unit time is greater than that in the case of complete combustion in which the equivalence ratio is 1.0. This will cause the relative content of oxygen gas required for complete combustion to decrease, resulting in insufficient combustion. In this case, incomplete combustion occurs, since there is not enough oxygen to allow methane to react completely in the burner. Therefore,

when the equivalence ratio is 1.0, higher temperatures can be achieved in the burner, associated with higher combustion performance.

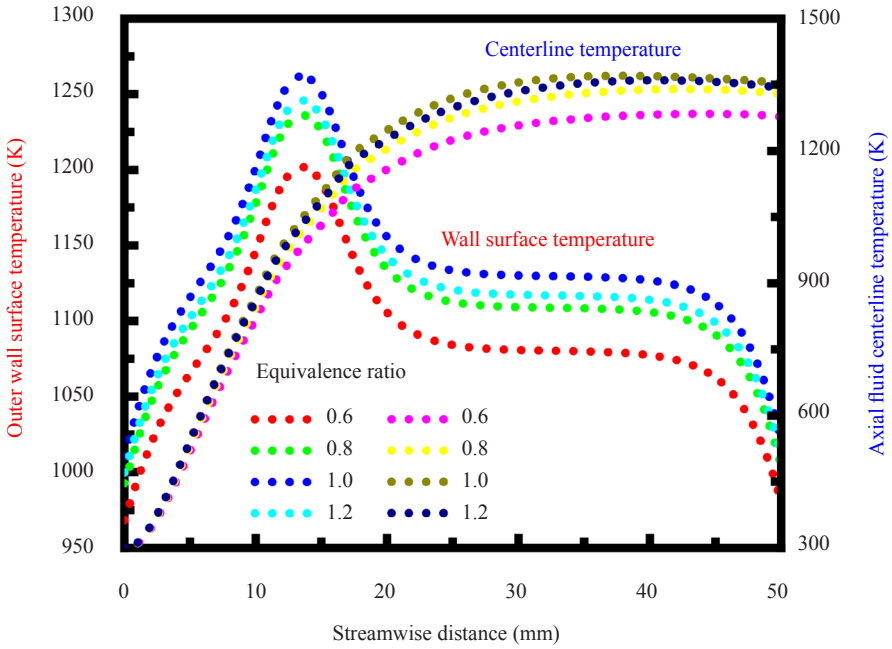

Figure 18. Temperature profiles along the outer wall surface of the burner and the axial fluid centerline under different wall heat transfer coefficient conditions

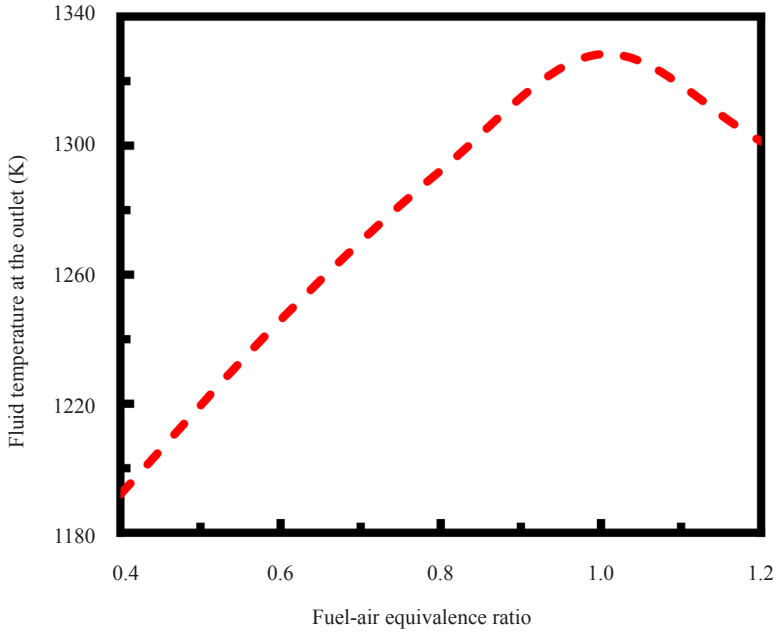

Figure 19. Axial centerline rate profiles of the combustion reaction under different wall heat transfer coefficient conditions

The effect of the equivalence ratio on the fluid temperature at the outlet is investigated. The results are presented

in Figure 19, in which the fluid temperature at the outlet is plotted against the equivalence ratio. The fluid temperature at the outlet indicates the enthalpy of flue gas. The equivalence ratio can be fuel-lean or fuel-rich. Combustion has been stabilized at an equivalence ratio as small as 0.4. With lean premixed combustion, the fuel-air equivalent ratio is smaller than 1.0. In this case, the fluid temperature at the outlet increases with the equivalent ratio of fuel to air, which increases the power output of the cavity-stabilized burner. The use of an equivalent ratio of 1.0 permits complete combustion of the fuel, and therefore there is an optimum condition of maximal temperature. However, there is a dominant loss that is caused by sensible heat leaving with the flue gas. When the fuel-air equivalent ratio is greater than 1.0, the fluid temperature at the outlet decreases with the equivalent ratio of fuel to air, which is primarily caused by the amount of methane gas flowing into the burner, as discussed above. In this case, the amount of air flowing into the burner is smaller than the amount of air required for complete combustion. Therefore, only a portion of the total fuel is reacted in the cavity-stabilized burner. For the fuel-rich case, there are issues of efficiency loss, since the equivalent ratio should be limited to allow sufficient air for combustion in the cavity-stabilized burner.

3.7 *Nusselt number analysis*

A dimensionless number analysis is performed to better understand the heat transfer characteristics of the burner. The Nusselt number or dimensionless heat transfer coefficient is evaluated at a specific streamwise distance. The Nusselt number is plotted in Figure 20 against the streamwise distance. Two entirely different cases are considered. In case A, the flame is stabilized near the entrance. In case B, the flame approaches blowout at a high flow velocity. The Nusselt number approaches 6 in both cases. However, the Nusselt number exhibits strongly non-monotonic behavior with an oscillation at the combustion region. This fingerprints the heat source, namely combustion chemistry downstream of the entrance heating the walls as well as walls upstream transferring heat to the cold incoming mixture.

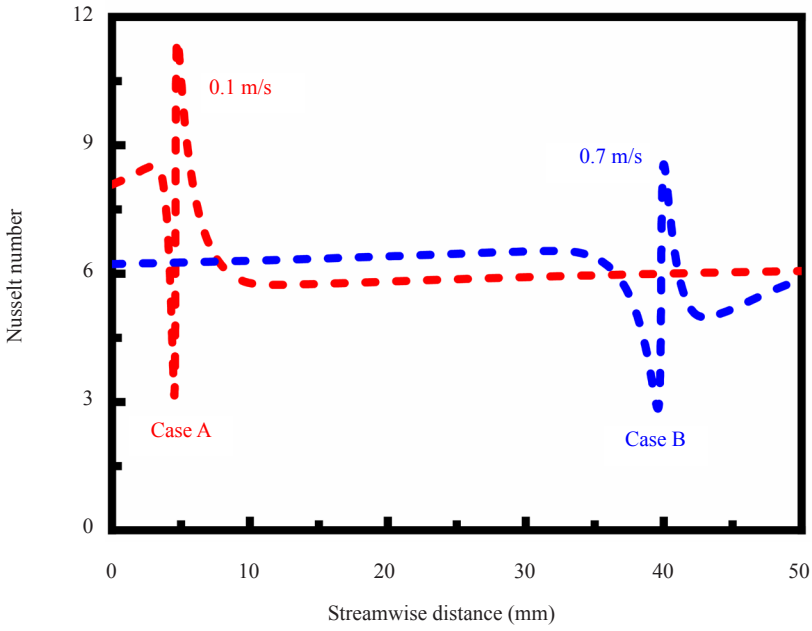

Figure 20. Nusselt number profiles along the axial direction under different inlet velocity conditions. In case A, the inlet velocity is 0.1 m/s. In case B, the inlet velocity is 0.7 m/s

4. Conclusions

Simulations are conducted to gain insights into burner performance such as reaction rates, species concentrations, temperatures, and flames. The factors affecting combustion characteristics are determined for the cavity-stabilized

burner. The major conclusions are summarized as follows:

• Combustion is stabilized and flame stability is improved by recirculation of hot combustion products induced by the cavity structure.

• The inlet velocity of the mixture is a critical factor in assuring flame stability within the cavity-stabilized burner. There is a narrow range of inlet velocities that permit sustained combustion within the cavity-stabilized burner. Fast flows can cause a blowout and slow flows can cause extinction. There exists an optimum inlet velocity for the greatest flame stability.

• The thermal conductivity of the burner walls plays a vital role in flame stability. Burner walls with low thermal conductivity will cause hot spots of high temperatures within the walls, which may lead to mechanical failure. In contrast, burner walls with high thermal conductivity are substantially isothermal and the burner has lower fluid centerline temperatures.

• Improvements in flame stability are achievable by using walls with anisotropic thermal conductivity. Such walls with anisotropic heat conduction properties will allow upstream heat flux to preheat the incoming mixture, yet not allow heat losses in the transverse direction.

• Combustion at the microscale can offer many advantages. Faster ignition and more efficient heat transfer can be achieved, but the design is challenging due to the loss of flame stability. Burners with large dimensions lead to a delay in flame ignition and may cause a blowout.

• Loss of flame stability due to external heat losses are main issues that require thermal management. Heat-insulating materials are favored to minimize external heat losses.

• The fuel-air equivalent ratio has a strong effect on flame stability. There are issues of efficiency loss for fuel-rich cases.

Conflict of interest

The author declares that there is no conflict of interest.

References

[1] R. S. Wegeng and M. K. Drost, "Developing new miniature energy systems," *Mechanical Engineering*, vol. 116, no. 9, pp. 82-85, 1994.

[2] T. A. Ameel, R. O. Warrington, R. S. Wegeng, and M. K. Drost, "Miniaturization technologies applied to energy systems," *Energy Conversion and Management*, vol. 38, no. 10-13, pp. 969-982, 1997.

[3] A. H. Epstein, "Millimeter-scale, micro-electro-mechanical systems gas turbine engines," *Journal of Engineering for Gas Turbines and Power*, vol. 126, no. 2, pp. 205-226, 2004.

[4] A. H. Epstein, Millimeter-scale, MEMS gas turbine engines," In Proceedings of the ASME Turbo Expo 2003, collocated with the 2003 International Joint Power Generation Conference, 2003, pp. 669-696.

[5] R. B. Peterson, "Small packages. Miniaturization technologies applied to energy systems," *Mechanical Engineering*, vol. 123, no. 6, pp. 58-61, 2001.

[6] S. Kota, G. K. Ananthasuresh, S. B. Crary, and K. D. Wise, "Design and fabrication of microelectromechanical systems," *Journal of Mechanical Design*, vol. 116, no. 4, pp. 1081-1088, 1994.

[7] S. A. Tadigadapa and N. Najafi, "Developments in microelectromechanical systems (MEMS): A manufacturing perspective," *Journal of Manufacturing Science and Engineering*, vol. 125, no. 4, pp. 816-823, 2003.

[8] G. K. Ananthasuresh and L. L. Howell, "Mechanical design of compliant microsystems-A perspective and prospects," *Journal of Mechanical Design*, vol. 127, no. 4, pp. 736-7383, 2005.

[9] J. Q. E, J. J. Ding, J. W. Chen, G. L. Liao, F. Zhang, and B. Luo, "Process in micro-combustion and energy conversion of micro power system: A review," *Energy Conversion and Management*, vol. 246, article number: 114664, 2021.

[10] J. Q. E, B. Luo, D. D. Han, J. W. Chen, G. L. Liao, F. Zhang, and J. J. Ding, "A comprehensive review on performance improvement of micro energy mechanical system: Heat transfer, micro combustion and energy conversion," *Energy*, vol. 239, no. E, article number: 122509, 2022.

[11] J. L. Wan and A. W. Fan, "Recent progress in flame stabilization technologies for combustion-based micro energy and power systems," *Fuel*, vol. 286, no. 2, article number: 119391, 2021.
[12] A. Gharehghani, K. Ghasemi, M. Siavashi, and S. Mehranfar, "Applications of porous materials in combustion systems: A comprehensive and state-of-the-art review," *Fuel*, vol. 304, article number: 121411, 2021.
[13] Y. G. Ju and K. Maruta, "Microscale combustion: Technology development and fundamental research," *Progress in Energy and Combustion Science*, vol. 37, no. 6, pp. 669-715, 2011.
[14] S. K. Chou, W. M. Yang, K. J. Chua, J. Li, and K. L. Zhang, "Development of micro power generators-A review," *Applied Energy*, vol. 88, no. 1, pp. 1-16, 2011.
[15] J. Kim, J. L. Yu, S. Lee, A. Tahmasebi, C.-H. Jeon, and J. Lucas, "Advances in catalytic hydrogen combustion research: Catalysts, mechanism, kinetics, and reactor designs," *International Journal of Hydrogen Energy*, vol. 46, no. 80, pp. 40073-40104, 2021.
[16] D. C. Walther and J. Ahn, "Advances and challenges in the development of power-generation systems at small scales," *Progress in Energy and Combustion Science*, vol. 37, no. 5, pp. 583-610, 2011.
[17] J. Miwa, Y. Asako, C. Hong, and M. Faghri, "Performance of gas-to-gas micro-heat exchangers," *Journal of Heat Transfer*, vol. 131, no. 5, article number: 051801, 2009.
[18] C. Marques and K. W. Kelly, "Fabrication and performance of a pin fin micro heat exchanger," *Journal of Heat Transfer*, vol. 126, no. 3, pp. 434-444, 2004.
[19] Z. Y. Zhao, Z. X. Zuo, W. Wang, N. L. Kuang, and P. Y. Xu, "Experimental studies on a high performance thermoelectric system based on micro opposed flow porous combustor," *Energy Conversion and Management*, vol. 253, article number: 115157, 2022.
[20] S. M. R. Sadatakhavi, S. Tabejamaat, M. E. A. Zade, B. Kankashvar, and M. R. Nozari, "Numerical and experimental study of the effects of fuel injection and equivalence ratio in a can micro-combustor at atmospheric condition," *Energy*, vol. 225, article number: 120166, 2021.
[21] J. Guan, X. J. Lv, C. Spataru, and Y. W. Weng, "Experimental and numerical study on self-sustaining performance of a 30-kW micro gas turbine generator system during startup process," *Energy*, vol. 236, article number: 121468, 2021.
[22] J. M. Seo, H.-S. Lim, J. Y. Park, M. R. Park, and B. S. Choi, "Development and experimental investigation of a 500-W class ultra-micro gas turbine power generator," *Energy*, vol. 124, pp. 9-18, 2017.
[23] I. A. Waitz, G. Gauba, and Y.-S. Tzeng. "Combustors for micro-gas turbine engines," *Journal of Fluids Engineering*, vol. 120, no. 1, pp. 109-117, 1998.
[24] C. M. Spadaccini, A. Mehra, J. Lee, X. Zhang, S. Lukachko, and I. A. Waitz, "High power density silicon combustion systems for micro gas turbine engines," *Journal of Engineering for Gas Turbines and Power*, vol. 125, no. 3, pp. 709-719, 2003.
[25] O. Dessornes, S. Landais, R. Valle, A. Fourmaux, S. Burguburu, C. Zwyssig, and Z. Kozanecki, "Advances in the development of a microturbine engine," *Journal of Engineering for Gas Turbines and Power*, vol. 136, no. 7, article number: 071201, 2014.
[26] M. Nozari, S. Tabejamaat, H. Sadeghizade, and M. Aghayari, "Experimental investigation of the effect of gaseous fuel injector geometry on the pollutant formation and thermal characteristics of a micro gas turbine combustor," *Energy*, vol. 235, article number: 121372, 2021.
[27] D. H. Lee, D.-E. Park, E. Yoon, and S. Kwon, "A MEMS piston-cylinder device actuated by combustion," *Journal of Heat Transfer*, vol. 125, no. 3, pp. 487-493, 2003.
[28] C. S. Cunningham, D. Ransom, J. Wilkes, J. Bishop, and B. White, "Mechanical design features of a small gas turbine for power generation in unmanned aerial vehicles," In Proceedings of ASME Turbo Expo 2015: Turbine Technical Conference and Exposition, 2015.
[29] N. S. Kaisare and D. G. Vlachos, "A review on microcombustion: Fundamentals, devices and applications," *Progress in Energy and Combustion Science*, vol. 38, no. 3, 2012, pp. 321-359.
[30] K. Maruta, "Micro and mesoscale combustion," *Proceedings of the Combustion Institute*, vol. 33, no. 1, pp. 125-150, 2011.
[31] D. Dunn-Rankin, E. M. Leal, and D. C. Walther, "Personal power systems," *Progress in Energy and Combustion Science*, vol. 31, no. 5-6, pp. 422-465, 2005.
[32] A. C. Fernandez-Pello, "Micropower generation using combustion: Issues and approaches," *Proceedings of the Combustion Institute*, vol. 29, no. 1, pp. 883-899, 2002.
[33] K. M. Lyons, "Toward an understanding of the stabilization mechanisms of lifted turbulent jet flames: Experiments," *Progress in Energy and Combustion Science*, vol. 33, no. 2, pp. 211-231, 2007.

[34] S. J. Shanbhogue, S. Husain, and T. Lieuwen, "Lean blowoff of bluff body stabilized flames: Scaling and dynamics," *Progress in Energy and Combustion Science*, vol. 35, no. 1, pp. 98-120, 2009.
[35] V. N. Kurdyumov and C. Jiménez, "Structure and stability of premixed flames propagating in narrow channels of circular cross-section: Non-axisymmetric, pulsating and rotating flames," *Combustion and Flame*, vol. 167, pp. 149-163, 2016.
[36] A. Dejoan, C. Jiménez, and V. N. Kurdyumov, "Critical conditions for non-symmetric flame propagation in narrow channels: Influence of the flow rate, the thermal expansion, the Lewis number and heat-losses," *Combustion and Flame*, vol. 209, pp. 430-440, 2019.
[37] C. M. Miesse, R. I. Masel, C. D. Jensen, M. A. Shannon, and M. Short, "Submillimeter-scale combustion," *AIChE Journal*, vol. 50, no.12, pp. 3206-3214, 2004.
[38] A. M. Mahuthannan, Y. Krishna, G. Magnotti, W. L. Roberts, and D. A. Lacoste, "Time-resolved thermometric investigation of flame quenching between parallel flat plates," *Fuel*, vol. 305, article number: 121511, 2021.
[39] K. Narukawa, Y. Minamoto, M. Shimura, and M. Tanahashi, "Near-wall flame propagation behaviour with and without surface reactions," *Fuel*, vol. 268, article number: 117216, 2020.
[40] Y. Fan, J. Q. Guo, M. Lee, N. Iki, and Y. Suzuki, "Quantitative evaluation of wall chemical effect in hydrogen flame using two-photon absorption LIF," *Proceedings of the Combustion Institute*, vol. 38, no. 2, pp. 2361-2370, 2021.
[41] K. T. Kim, D. H. Lee, and S. Kwon, "Effects of thermal and chemical surface-flame interaction on flame quenching," *Combustion and Flame*, vol. 146, no. 1-2, pp. 19-28, 2006.
[42] S. R. Lin, H. Yuan, and X. Y. Huang, "A computational study on the quenching and near-limit propagation of smoldering combustion," *Combustion and Flame*, vol. 238, article number: 111937, 2022.
[43] M. H. Wang, P. F. Li, and F. F. Wang, "Dependence of the blowout limit on flow structure, heat transfer, and pressure loss in a bluff-body micro-combustor," *International Journal of Hydrogen Energy*, vol. 45, no. 38, pp. 19912-19925, 2020.
[44] J. L. Wan and H. B. Zhao, "Blowout limit of premixed flame in a micro preheated combustor with a flame holder at different blockage ratios," *International Journal of Hydrogen Energy*, vol. 45, no. 46, pp. 25468-25478, 2020.
[45] J. Choi, W. Lee, R. Rajasegar, T. Lee, and J. Yoo, "Effects of hydrogen enhancement on mesoscale burner array flame stability under acoustic perturbations," *International Journal of Hydrogen Energy*, vol. 46, no. 74, pp. 37098-37107, 2021.
[46] K. R. McManus, T. Poinsot, and S. M. Candel, "A review of active control of combustion instabilities," *Progress in Energy and Combustion Science*, vol. 19, no. 1, pp. 1-29, 1993.
[47] R. Sadanandan, A. Chakraborty, V. K. Arumugam, and S. R. Chakravarthy, "Partially premixed flame stabilization in the presence of a combined swirl and bluff body influenced flowfield: An experimental investigation," *Journal of Engineering for Gas Turbines and Power*, vol. 142, no. 7, article number: 071010, 2020.
[48] K. M. Kundu, D. Banerjee, and D. Bhaduri, "On flame stabilization by bluff-bodies," *Journal of Engineering for Gas Turbines and Power*, vol. 102, no. 1, pp. 209-214, 1980.
[49] C. C. Rasmussen, J. F. Driscoll, K.-Y. Hsu, J. M. Donbar, M. R. Gruber, and C.D. Carter, "Stability limits of cavity-stabilized flames in supersonic flow," *Proceedings of the Combustion Institute*, vol. 30, no. 2, pp. 2825-2833, 2005.
[50] N. Kato and S.-K. Im, "Flame dynamics under various backpressures in a model scramjet with and without a cavity flameholder," *Proceedings of the Combustion Institute*, vol. 38, no. 3, pp. 3861-3868, 2021.
[51] S. X. Wang and A. W. Fan, "Combustion regimes of syngas flame in a micro flow reactor with controlled temperature profile: A numerical study," *Combustion and Flame*, vol. 230, article number: 111457, 2021.
[52] S. L. Ni, D. Zhao, Y. C. You, Y. Huang, B. Wang, and Y. P. Su, "NOx emission and energy conversion efficiency studies on ammonia-powered micro-combustor with ring-shaped ribs in fuel-rich combustion," *Journal of Cleaner Production*, vol. 320, article number: 128901, 2021.
[53] C. K. Westbrook and F. L. Dryer, "Simplified reaction mechanisms for the oxidation of hydrocarbon fuels in flames," *Combustion Science and Technology*, vol. 27, no. 1-2, pp. 31-43, 1981.
[54] C. K. Westbrook and F. L. Dryer, "Chemical kinetic modeling of hydrocarbon combustion," *Progress in Energy and Combustion Science*, vol. 10, no. 1, pp. 1-57, 1984.
[55] M. Barrère and F. A. Williams, "Comparison of combustion instabilities found in various types of combustion chambers," *Symposium (International) on Combustion*, vol. 12, no. 1, 1969, pp. 169-181.
[56] F. A. Williams, "Theory of combustion in laminar flows," *Annual Review of Fluid Mechanics*, vol. 3, pp. 171-188, 1971.
[57] J. Buckmaster, "The structure and stability of laminar flames," *Annual Review of Fluid Mechanics*, vol. 25, pp. 21-

53, 1993.
[58] P. Clavin, "Premixed combustion and gasdynamics," *Annual Review of Fluid Mechanics*, vol. 26, pp. 321-352, 1994.
[59] G. I. Sivashinsky, "Instabilities, pattern formation, and turbulence in flames," *Annual Review of Fluid Mechanics*, vol. 26, pp. 321-352, 1994.
[60] M. Matalon, "Intrinsic flame instabilities in premixed and nonpremixed combustion," *Annual Review of Fluid Mechanics*, vol. 39, pp. 163-191, 2007.
[61] C. M. Vagelopoulos, F. N. Egolfopoulos, and C. K. Law, "Further considerations on the determination of laminar flame speeds with the counterflow twin-flame technique," *Symposium (International) on Combustion*, vol. 25, no. 1, pp. 1341-1347, 1994.
[62] C. M. Vagelopoulos and F. N. Egolfopoulos, "Direct experimental determination of laminar flame speeds," *Symposium (International) on Combustion*, vol. 27, no. 1, pp. 513-519, 1998.
[63] D. G. Norton and D. G. Vlachos, "Combustion characteristics and flame stability at the microscale: A CFD study of premixed methane-air mixtures," *Chemical Engineering Science*, vol. 58, no. 21, pp. 4871-4882, 2003.
[64] D. G. Norton and D. G. Vlachos, "A CFD study of propane-air microflame stability," *Combustion and Flame*, vol. 138, no. 1-2, pp. 97-107, 2004.
[65] T. T. Leach and C. P. Cadou, "The role of structural heat exchange and heat loss in the design of efficient silicon micro-combustors," *Proceedings of the Combustion Institute*, vol. 30, no. 2, pp. 2437-2444, 2005.
[66] T. T. Leach, C. P. Cadou, and G. S. Jackson, "Effect of structural conduction and heat loss on combustion in micro-channels," *Combustion Theory and Modelling*, vol. 10, no. 1, pp. 85-103, 2006.
[67] C.-H. Chen and P. D. Ronney, "Scale and geometry effects on heat-recirculating combustors," *Combustion Theory and Modelling*, vol. 17, no. 5, pp. 888-905, 2013.
[68] N. S. Kaisare and D. G. Vlachos, "Optimal reactor dimensions for homogeneous combustion in small channels," *Catalysis Today*, vol. 120, no. 1, pp. 96-106, 2007.
[69] X. F. Xu, L. F. C. Pereira, Y. Wang, J. Wu, K. W. Zhang, X. M. Zhao, S. Bae, C. T. Bui, R. G. Xie, J. T. L. Thong, B. H. Hong, K. P. Loh, D. Donadio, B. W. Li, and B. Özyilmaz, "Length-dependent thermal conductivity in suspended single-layer graphene," *Nature Communications*, vol. 5, article number: 3689, 2014.
[70] Z. Y. Wei, Z. H. Ni, K. D. Bi, M. H. Chen, and Y. F. Chen, "In-plane lattice thermal conductivities of multilayer graphene films," *Carbon*, vol. 49, no. 8, pp. 2653-2658, 2011.
[71] W. Liu, L. Wang, S. C. Su, Z. Z. Wu, Y. S. Guo, and K. D. Du, "Study of the flame flow and combustion characteristics of pool fires around a bluff body in the ship engine room," *Case Studies in Thermal Engineering*, vol. 28, article number: 101514, 2021.
[72] Y. K. Huang, X. M. He, Y. Jin, H. Y. Zhu, and Z. X. Zhu, "Effect of non-uniform inlet profile on the combustion performance of an afterburner with bluff body," *Energy*, vol. 216, article number: 119142, 2021.
[73] Y. F. Yan, G. G. Wu, W. P. Huang, L. Zhang, L. X. Li, and Z. Q. Yang, "Numerical comparison study of methane catalytic combustion characteristic between newly proposed opposed counter-flow micro-combustor and the conventional ones," *Energy*, vol. 170, pp. 403-410, 2019.
[74] J. M. Rodrigues, M. F. Ribeiro, and E. C. Fernandes, "Catalytic activity of electrodeposited cobalt oxide films for methane combustion in a micro-channel reactor," *Fuel*, vol. 232, pp. 51-59, 2018.
[75] J. A. Miller and C. T. Bowman, "Mechanism and modeling of nitrogen chemistry in combustion," *Progress in Energy and Combustion Science*, vol. 15, no. 4, pp. 287-338, 1989.
[76] P. Glarborg, J. A. Miller, B. Ruscic, and S. J. Klippenstein, "Modeling nitrogen chemistry in combustion," *Progress in Energy and Combustion Science*, vol. 67, pp. 31-68, 2018.